catalysts

MDPI

Article

HDO of Methyl Palmitate over Silica-Supported Ni Phosphides: Insight into Ni/P Effect

Irina V. Deliy *, Ivan V. Shamanaev, Evgeny Yu. Gerasimov, Vera P. Pakharukova, Ilya V. Yakovlev, Olga B. Lapina, Pavel V. Aleksandrov and Galina A. Bukhtiyarova

Boreskov Institute of Catalysis, Pr. Lavrentieva 5, 630090 Novosibirsk, Russia; i.v.shamanaev@catalysis.ru (I.V.S.); gerasimov@catalysis.ru (E.Y.G.); verapakharukova@yandex.ru (V.P.P.); spitzstichel@gmail.com (I.V.Y.); olga@catalysis.ru (O.B.L.); aleksandrov@catalysis.ru (P.V.A.); gab@catalysis.ru (G.A.B.)

* Correspondence: delij@catalysis.ru; Tel.: +7-383-326-9410

Academic Editor: Yong-Kul Lee and Keith Hohn

Received: 30 July 2017; Accepted: 30 September 2017; Published: 4 October 2017

Abstract: Two sets of silica-supported nickel phosphide catalysts with a nickel content of about 2.5 and 10 wt % and Ni/P molar ratio 2/1, 1/1 and 1/2 in each set, were prepared by way of a temperature-programmed reduction method using ($Ni(CH_3COO)_2$) and ($(NH_4)_2HPO_4$) as a precursor. The Ni_xP_y/SiO_2 catalysts were characterized using chemical analysis N_2 physisorption, XRD, TEM, ^{31}P MAS NMR. Methyl palmitate hydrodeoxygenation (HDO) was performed in a trickle-bed reactor at 3 MPa and 290 °C with LHSV ranging from 0.3 to 16 h^{-1}. The Ni/P ratio was found to affect the nickel phosphide phase composition, PO_x groups content and catalytic properties in methyl palmitate HDO with the TOF increased along with a decline of Ni/P ratio and a growth of PO_x groups' content. Taking into account the possible routes of methyl palmitate conversion (metal-catalyzed hydrogenolysis or acid-catalyzed hydrolysis), we proposed that the enhancement of acid PO_x groups' content with the Ni/P ratio decrease provides an enhancement of the rate of methyl palmitate conversion through the acceleration of acid-catalyzed hydrolysis.

Keywords: nickel phosphide; Ni/P ratio; nickel content; PO_x groups content; ^{31}P MAS NMR; acidity; hydrodeoxygenation; methyl palmitate

1. Introduction

Triglyceride-based feedstocks are widely studied as a resource for the production of diesel-range or aviation fuel through the hydrodeoxygenation (HDO) process using aliphatic ether or acid as model compounds [1–5]. HDO of triglycerides, fatty esters and acids produce an oxygen-free mixture of alkanes which are the valuable components compatible with petroleum-based motor fuels [6]. In recent years transition metal phosphide systems have proved to be the promising catalysts in HDO of fatty acid methyl esters [7–16], fatty acids [17] and vegetable oils [5,18] as well as in co-hydroprocessing of vegetable oils and gas oil mixture [19]. Among a number of transition metal phosphides the silica-supported nickel phosphide catalysts were found to display a higher activity in HDO of aliphatic ether [7], which is converted through the complicated scheme with the participation of acid-catalyzed and metal-catalyzed reactions [7,12,14,15,20,21]. Alkanes with the same number of carbon atoms and water are produced in the HDO pathways including hydrogenation-dehydrogenation and dehydration reactions; while $DeCO_x$ pathways produce alkanes with shorter carbon chains and CO_x molecules via hydrogenolysis of C-C bonds.

The catalytic activities of nickel phosphides in hydrogenation and hydrogenolysis reactions are attributed to their metallic and acidic properties [12,22–25], caused by the covalent nature of Ni-P bond in phosphides and a slight charge transfer from Ni to P [25]. Metal phosphides contain weak

Brønsted and Lewis acid sites attributed to the presence of unreduced PO_x groups and the metal sites with small positive charge, respectively [7,26–28]. The various aspects of preparation technique, such as precursor nature, reduction temperature, metal content and Ni/P ratio were observed to affect the physicochemical and catalytic properties of the Ni_xP_y/SiO_2 catalyst [24,29–32].

It was stated that the initial Ni/P molar ratio has a profound effect on the structure and catalytic activity of the supported nickel phosphide catalysts obtained with a conventional preparation method by temperature-programmed reduction (TPR) of nickel phosphate precursors [7,8,12,17,18,29,31,33]. Stinner et al. [29] have reported that Ni/P molar ratio equal to 2 leads to the formation of $Ni_{12}P_5$ and Ni_3P phases over silica, Ni/P molar ratio equal to 1.7 leads to $Ni_{12}P_5$ and Ni_2P phases, and Ni/P molar ratio = 1.5 favors Ni_2P phase only.

Chen et al. [7] studied the silica-supported nickel phosphide catalysts with different Ni/P molar ratios in methyl laurate HDO. It was observed that the catalytic activity of obtained catalysts followed the order:

$$Ni_3P\ (Ni/P = 3/1) < Ni_{12}P_5\ (Ni/P = 2/1) < Ni_2P\ (Ni/P = 1/1 \text{ and } 1/2) \approx Ni.$$

Yang et al. [8] investigated the influence of Ni/P molar ratios on the performance of Ni_xP_y/SBA-15 catalysts in methyl oleate HDO. It was shown that Ni_2P/SBA-15 catalyst with Ni/P = 1/1 presents the highest catalytic activity; the catalytic activity of nickel phosphide catalysts in methyl oleate HDO followed the order:

$$Ni_3P\ (Ni/P = 3/1) < Ni_{12}P_5\ (Ni/P = 2/1) \approx Ni_2P\ (Ni/P = 1/2) < Ni_2P\ (Ni/P = 1/1).$$

It was mentioned that the catalytic activity of Ni/SBA-15 catalyst is slightly higher than demonstrated by any of the similar prepared Ni_2P/SBA-15 samples in methyl oleate HDO [8,9]. Guan et al. [10] and Xue et al. [11] showed the opposite results on methyl palmitate HDO in the presence of Ni/SiO_2 and Ni_2P/SiO_2 catalysts. It was pointed [10] that Ni_2P/SiO_2 showed significantly higher activity in comparison with Ni/SiO_2 in terms of methyl palmitate conversion. The catalytic activity of the Ni_xP_y/SiO_2 catalysts depending on Ni/P ratios increases in the order:

$$Ni_2P\ (Ni/P = 1/1.5) < Ni_2P\ (Ni/P = 1/1.75) < Ni_2P\ (Ni/P = 1/2) < Ni_2P \text{ and } Ni_5P_4\ (Ni/P = 1/2.5).$$

The above-cited articles demonstrate discrepancy in the results concerning the effect of Ni/P ratio on the catalytic properties of nickel phosphide catalysts in methyl ethers HDO. Nearly the same activities in methyl laurate HDO were reported by Chen et al. [7] for the catalysts with the Ni/P ratios 1/1 and 1/2 indicating negligible effect at Ni/P < 1; according to Yang et al. [8] the highest activity in methyl oleate HDO was displayed by the catalyst with Ni/P = 1/1. And, finally, a gradual increase in catalytic activity was observed in the study of Guan at el. [10] with the decrease of Ni/P ratio from 1/1.15 to 1/2.5. This discrepancy can be explained by the use of catalysts with the different metal loading, mean particle sizes or wide particle size distribution, which could have influenced the catalytic activity. The scarce data on size effect are also rather contradictory. According to data reported by Guan et al. [13] the particle size increase of MCM-41 supported nickel phosphide has no influence on TOF of methyl palmitate conversion. Yang et al. [14] reported that the TOF increased with the Ni_2P crystallite size in the methyl laurate HDO.

To reach a better insight into the Ni/P effect on the catalytic properties of silica-supported nickel phosphide catalysts in methyl palmitate HDO two sets of Ni_xP_y/SiO_2 catalysts differing in Ni content and Ni/P ratio were used in the present study [15]. The low-loaded catalysts (about 2.5 wt % of nickel) with nearly the same mean particle size are the appropriate candidates for the comparison of specific activities of the Ni_xP_y/SiO_2 catalysts with the Ni/P ratios 2:1, 1:1 and 1:2. The high-loaded samples (about 9–10 wt % of nickel) were used to follow the evolution of the active phase with the

Ni/P decrease the X-Ray Diffraction (XRD), transmission electron microscopy (TEM) and P^{31} nuclear magnetic resonance (NMR) techniques were employed.

2. Results and Discussion

2.1. Catalysts Characterization

Two sets of the Ni_xP_y/SiO_2 catalysts were prepared with different initial Ni/P molar ratios and nickel content in each series in the range of 2.5–2.9 wt % (denoted as low-loaded samples, *l*-Ni_xP_y) or 9.0–10.9 wt % (denoted as high-loaded samples, *h*-Ni_xP_y). For the preparation of each set of the catalysts the solutions of nickel acetate ($Ni(CH_3COO)_2$) and di-ammonium hydrogen phosphate ($(NH_4)_2HPO_4$) were used, containing the adjusted amount of Ni and different initial Ni/P molar ratios of 2/1; 1/1 or 1/2. The obtained samples were denoted as *h*-Ni2P1, *h*-Ni1P1, *h*-Ni1P2 and *l*-Ni2P1, *l*-Ni1P1, *l*-Ni1P2, correspondingly.

Recently Shamanaev et al. [16] established the optimal reduction conditions for the silica-supported nickel phosphide catalysts displaying the highest catalytic activity in methyl palmitate hydrodeoxygenation. On the basis of our previous results [15,16] and the literature data reported for the phosphate-containing type of precursors [13,34–36] the reduction temperature of 600 °C was chosen in this study for catalysts preparation. The physicochemical properties of the Ni_xP_y/SiO_2 catalysts as well as PO_x/SiO_2 reference sample, and SiO_2 support are summarized in Table 1.

Table 1. Physicochemical properties of Ni_xP_y/SiO_2 catalysts as well as the reference samples Ni/SiO_2, PO_x/SiO_2 and SiO_2 support.

Sample	Ni, wt %	P, wt %	Ni/P Molar Ratio after TPR	A_{BET}, m^2/g	D_{pore}, nm	D_S after TPR, nm	X-ray Diffraction (XRD) Phase
SiO_2	-	-	-	300	10.6	-	-
PO_x/SiO_2	-	5.31	-	200	10.8	-	-
h-Ni	8.6	-	-	215	10.5		Ni
h-Ni2P1	10.9	2.4	2.4	195	11.7		$Ni_{12}P_5$
h-Ni1P1	10.3	3.6	1.5	190	10.4		Ni_2P
h-Ni1P2	9.0	5.0	0.9	175	10.3		Ni_2P
l-Ni2P1	2.9	0.8	2.1	290	10.1	4.9 ± 1.3	$Ni_{12}P_5$
l-Ni1P1	2.8	1.4	1.1	270	10.3	4.7 ± 1.1	Ni_2P
l-Ni1P2	2.5	1.9	0.7	255	10.5	3.5 ± 0.9	Ni_2P

According to the elemental analysis by ICP-AES, the Ni content in reduced samples varied from 2.5 to 2.9 wt % for the low-loaded set of samples (*l*-Ni_xP_y) and from 8 to 11 wt % for the high- loaded set of samples (*h*-Ni_xP_y). It was stated that the Ni/P molar ratios in reduced catalysts were higher than the initial Ni/P molar ratios in oxide precursors and impregnating solutions. The increase of the Ni/P molar ratio in the samples after reduction is caused by the formation of volatile phosphorus-containing species (namely PH_3, P, P_2 etc.) during high-temperature reduction as it has been reported earlier [31].

The textural parameters of the reduced catalysts have been obtained from the N_2 adsorption-desorption isotherms (Table 1). The BET specific surface areas (A_{BET}) of the low-loaded set of samples decrease slightly with nickel phosphide loading in comparison with the pure SiO_2 support (255–290 m^2/g vs. 300 m^2/g of SiO_2); the decrease of the BET surface areas for the high-loaded set of samples is more pronounced (175–195 m^2/g), indicating the partial coverage and/or clogging of the inner pore space of the catalysts by the nickel phosphide particles and residues of the phosphorus-containing compounds (unreduced PO_x groups [30,37], elemental P_4 and P_2 [29]). It was observed that with decreasing of the Ni/P ratio in each set of the reduced catalysts, the surface area and pore volume tended to decrease because of the surplus phosphorus-containing species on

silica surface [29,38]. The average pore diameters for the *l*-Ni_xP_y and *h*-Ni_xP_y sets of catalysts do not changed noticeably (Table 1).

The formation of nickel phosphide particles on silica surface after temperature-programmed reduction (TPR) was proved by XRD, TEM and ^{31}P-MAS NMR methods. The X-ray diffraction patterns of reduced Ni_xP_y/SiO_2 catalysts and SiO_2 support are presented in Figure 1. XRD pattern of the initial SiO_2 support (Figure 1a) contains a broad peak centered at 2θ ~22°, which corresponds to amorphous SiO_2 and can be seen in all of the represented XRD patterns of the Ni_xP_y/SiO_2 catalysts. Figure 1a shows the XRD patterns of the high-loaded *h*-Ni2P1 and low-loaded *l*-Ni2P1 samples that were prepared to start with the initial Ni/P molar ratio equal to 2/1. Apart from the diffraction peak related to the support, the characteristic peaks at 2θ = 32.6°, 38.4°, 41.7°, 44.4°, 46.9°and 48.9° of the $Ni_{12}P_5$ phase (a = b = 8.646 Å, c = 5.070 Å, α = β = γ = 90°; JCPDS #22-1190) are fixed in the diffraction patterns of Ni2P1 samples. The estimation of $Ni_{12}P_5$ crystallites size (D_{XRD}) on the surface of the high-loaded *h*-Ni2P1 sample gives about 16.0 nm, whereas the XRD pattern of low-loaded *l*-Ni2P1 sample contains very weak and broadened reflections from $Ni_{12}P_5$ phase, suggesting that this phase should be highly dispersed (Figure 1a). That makes difficult the correct determination of D_{XRD} for *l*-Ni2P1 sample.

Figure 1b shows the XRD patterns of the high-loaded *h*-Ni1P1 and low-loaded *l*-Ni1P1 samples prepared with equimolar initial Ni/P ratio. All of represented XRD patterns of Ni1P1 catalysts contain the characteristic peaks at 2θ = 40.6°, 44.5°, 47.1°, 54.1°, 54.8°, 66.1°, 72.5°and 74.5° of the Ni_2P phase (a = b = 5.859 Å, c = 3.382 Å, α = β = 90°, γ = 120°; JCPDS #03-0953) with D_{XRD} = 13 nm for *h*-Ni1P1 sample. The XRD patterns of the high-loaded *h*-Ni1P2 and low-loaded *l*-Ni1P2 samples prepared with the lower initial molar Ni/P = 1/2 are displayed in Figure 1c. The Ni_2P phase characteristic peaks are revealed in the diffraction patterns of Ni1P2 samples with the estimated Ni_2P crystallites size equal to D_{XRD} = 10 nm in the *h*-Ni1P2 sample. The diffraction patterns corresponding to *l*-Ni1P2 samples exhibits the broadened diffraction lines with a lower intensity indicating the presence of the highly dispersed Ni_2P phase. Also, as for the other low-loaded samples, it is hardly possible to estimate D_{XRD} for *l*-Ni1P2 sample from the XRD data correctly.

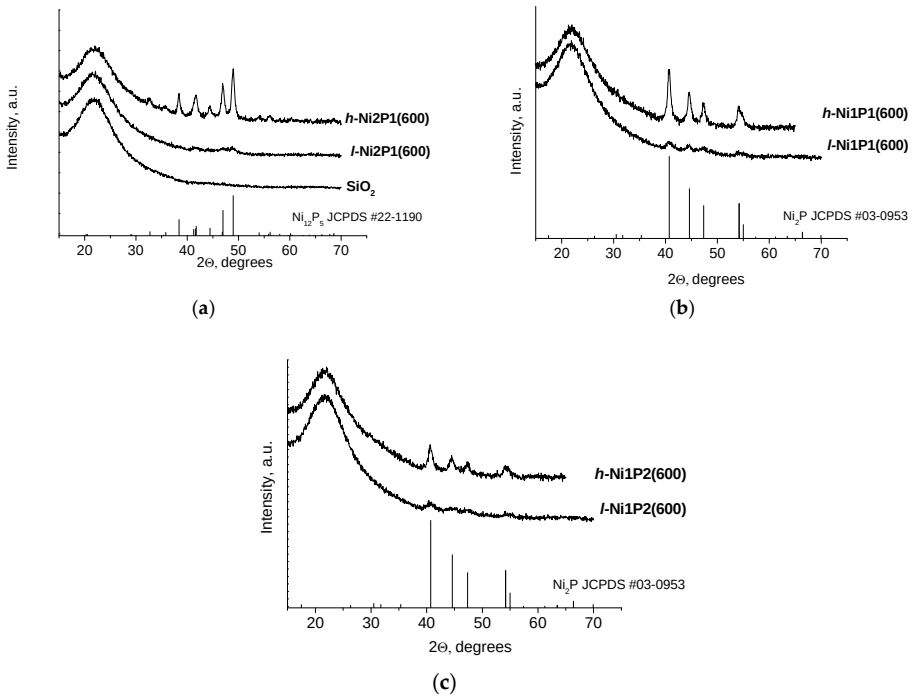

Figure 1. XRD patterns of silica-supported Ni_xP_y catalysts and SiO_2 support: (**a**) *h*-Ni2P1, *l*-Ni2P1 and SiO_2; (**b**) *h*-Ni1P1 and *l*-Ni2P1; (**c**) *h*-Ni1P2, *l*-Ni1P2.

Thus, the XRD data are shown in Table 1 and Figure 1 clearly demonstrate that the initial Ni/P molar ratio influences crystalline phase composition of the reduced phosphide catalysts. The initial Ni/P molar ratio of 2/1 favors formation of $Ni_{12}P_5$ phase. Further increasing the amount of phosphorus to Ni/P = 1/1 and 1/2 led to the formation of the Ni_2P phase. A similar dependence of nickel phosphide crystalline phase on the initial Ni/P molar ratio for silica-supported nickel phosphide catalysts has been observed previously for phosphate precursor [7,8,37,38]. The initial excess of P content in the precursors was shown to be the prerequisite of the Ni_2P phase formation [7,8,30,31,37,38].

The increase of phosphorus precursor content in the Ni_2P/SiO_2 catalysts leads to a higher dispersion of nickel phosphide particles on a silica support. The nickel phosphide crystallite sizes for the high-loaded set of the samples diminishes in the row: *h*-Ni2P1 (16.0 nm) > *h*-Ni1P1 (13.0 nm) > *h*-Ni1P2 (10.0 nm). Probably the initial nickel phosphate precursor was surrounded with an excess of polymeric phosphate species preventing the aggregation during the calcination step and favoring the higher dispersion of resulting nickel phosphide particles [31].

The TEM images of two sets of the Ni_xP_y/SiO_2 catalysts with different initial Ni/P molar ratios are shown in Figure 2a–f. The nickel phosphide particles with different size ranged in the regions from 2.0 to 20 nm were observed in the high-loaded *h*-Ni2P1, *h*-Ni1P1 and *h*-Ni1P2 samples (Figure 2a–c). Besides, several particles with the size up to 50 nm were found. The observed wide particle size distribution makes it difficult to estimate correctly the average size of particles by statistical analysis of the TEM patterns of *h*-Ni_xP_y samples. The TEM images of the low-loaded *l*-Ni2P1, *l*-Ni1P1, and *l*-Ni1P2 catalysts (Figure 2d–f) show the nickel phosphide particles with a narrow particle size distribution; the mean particle surface diameters (D_s) are 4.9 $\pm$ 1.3 nm for *l*-Ni2P1, 4.7 $\pm$ 1.1 nm for *l*-Ni1P1 and 3.5 $\pm$ 0.9 nm for *l*-Ni1P2. The TEM image of *l*-Ni2P1 sample (see Figure S1a in Supplementary Materials) reveals crystal lattice fringes with the d-spacing value of 2.20 Å, 2.47 Å, and 2.74 Å corresponding to the (202), (112) and (220) reflections of the $Ni_{12}P_5$ phase (JCPDS #22-1190), respectively. The TEM images of *l*-Ni1P1 and *l*-Ni1P2 samples in Figures S1b and S1c in Supplementary Materials exhibit crystal lattice fringes with the d-spacing value of 2.24 Å, 2.05 Å, and 1.92 Å corresponding to the (111), (201), and (120) reflections of the Ni_2P crystalline phase (JCPDS #03-0953).

To explore the nature of the phosphorus species on the reduced nickel phosphide catalysts the ^{31}P MAS NMR technique was employed. Prior to NMR experiments, nickel phosphide catalysts after reduction by the conventional TPR procedure at 600 °C were transferred into ampoules and further to NMR rotor in a glove box under argon atmosphere to avoid the contact with air. This technique helps to avoid possible oxidation of nickel phosphide during NMR spectra acquisition. Figure 3 demonstrates a spin-echo ^{31}P 14 kHz MAS NMR spectra of the high-loaded *h*-Ni2P1, *h*-Ni1P1 and *h*-Ni1P2 catalysts with different initial Ni/P molar ratio. Two main regions of the spectra of all the measured nickel phosphide catalysts can be highlighted. The first region from +500 to +5000 ppm corresponds to Ni-P intermetallic compounds such as $Ni_{12}P_5$, Ni_3P, Ni_2P, NiP, and Ni_5P_4 [15,29,39] and the second one from +4 to −40 ppm corresponds to the different phosphate species (denoted in this study overall as PO_x groups), i.e., phosphoric acid $H_nPO_4^{(3-n)-}$ (~0 ppm), terminal $P_2O_7^{4-}$ (~−7 ppm), and internal $(PO_3^-)_n$ (~−22 ppm) phosphate groups in phosphoric acid oligomers [15,29,32,40,41]. For all of the applied catalysts, we detected the lack of the signals with chemical shifts from −30 to −50 ppm that could be attributed to phosphorus-containing species in the form of silicon phosphate [40].

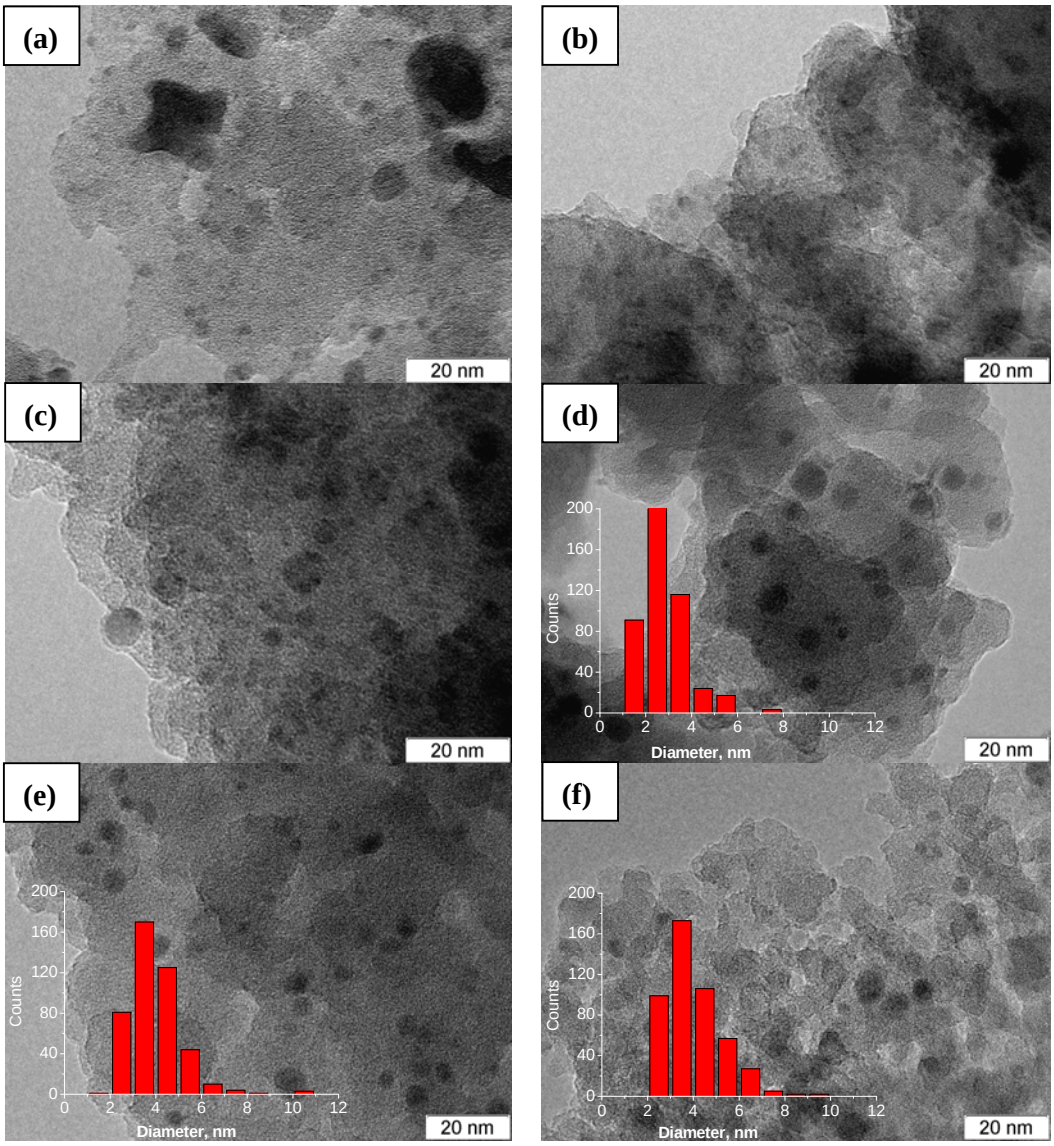

Figure 2. TEM images of Ni_xP_y/SiO_2 catalysts with different initial molar Ni/P ratio: (**a**) *h*-Ni2P1; (**b**) *h*-Ni1P1; (**c**) *h*-Ni1P2; (**d**) *l*-Ni2P1; (**e**) *l*-Ni1P1; (**f**) *l*-Ni1P2.

The ^{31}P NMR spectrum of *h*-Ni2P1 sample in Figure 3 shows two well-resolvable signals with isotropic chemical shifts at ~1950 and ~2250 ppm corresponding to $Ni_{12}P_5$ phase [29]. This observation agrees with the crystalline structure identified by XRD (Table 1). Also, the additional signals from other Ni-P intermetallic compounds at 900–1500 ppm chemical shifts region are revealed in the spectrum of *h*-Ni2P1 sample. However, the amount of this new phase is negligible (since the exact line shape of $Ni_{12}P_5$ is not known the precise ratio cannot be extracted). The amount of the phosphorus species in the form of PO_x groups ($\omega(PO_x)$) was determined from the intensities of signals in the chemical shifts region from +4 to −40 ppm. It was found that $\omega(PO_x) = 3.5$ at % for *h*-Ni2P1 sample.

The Ni_2P structure contains two crystallographic P sites and consequently gives two resonances with isotropic chemical shifts of 1487 and 4076 ppm [29]. The ^{31}P NMR spectra of *h*-Ni1P1 and *h*-Ni1P2 samples in Figure 3 show two signals with isotropic chemical shifts at ~1500 and ~4050 ppm, confirming the Ni_2P phase formation. The observed broad signal with a maximum at ~1500 ppm is not symmetric, most probably due to the superposition of several signals, the NMR line shape effects could also be a reason. The maximum at ~1500 ppm is most likely to corresponds to Ni_2P phase; nevertheless, the presence of other Ni-P intermetallic compounds as $Ni_{12}P_5$, Ni_3P, NiP, and Ni_5P_4 [29,39] cannot be

avoided since their chemical shifts lie in the same region and the large full width at a half maximum (FWHM) does not provide good separation of the lines. The large FWHM can be a result of either small particle or inhomogeneous character (defectiveness) of Ni-P intermetallic compounds.

The *h*-Ni1P1 sample shows two different phosphorus sites of Ni_2P in contrast to *h*-Ni1P2 sample for which both the lines are highly broadened. The downfield line shoulder is not observed in *h*-Ni1P1 sample either. Moreover, the line FWHM is narrower, which causes observation of spinning sidebands. It was found that the characteristic lines at ~1500 and ~4050 ppm in ^{31}P NMR spectrum of *h*-Ni1P1 sample are narrower than those for *h*-Ni1P2 sample probably because of smaller amount of stacking faults in *h*-Ni1P1 sample or larger average nickel phosphide particle size that leads to presence of some amount of large particles with well-formed Ni_2P phase giving rise to sharp peaks on the spectrum. The estimated values of $\omega(PO_x)$ are equal to 10.0 and 13.0 at % of total phosphorus for *h*-Ni1P1 and for *h*-Ni1P2 samples correspondingly. It is necessary to mention that ^{31}P NMR spectrum of low-loaded *l*-NiP2 sample resembles the spectrum of *h*-Ni1P2 catalyst, but intensities of the peaks in the low-loaded sample are noticeably lower, which makes questionable the quantitative estimation of the amount of PO_x groups.

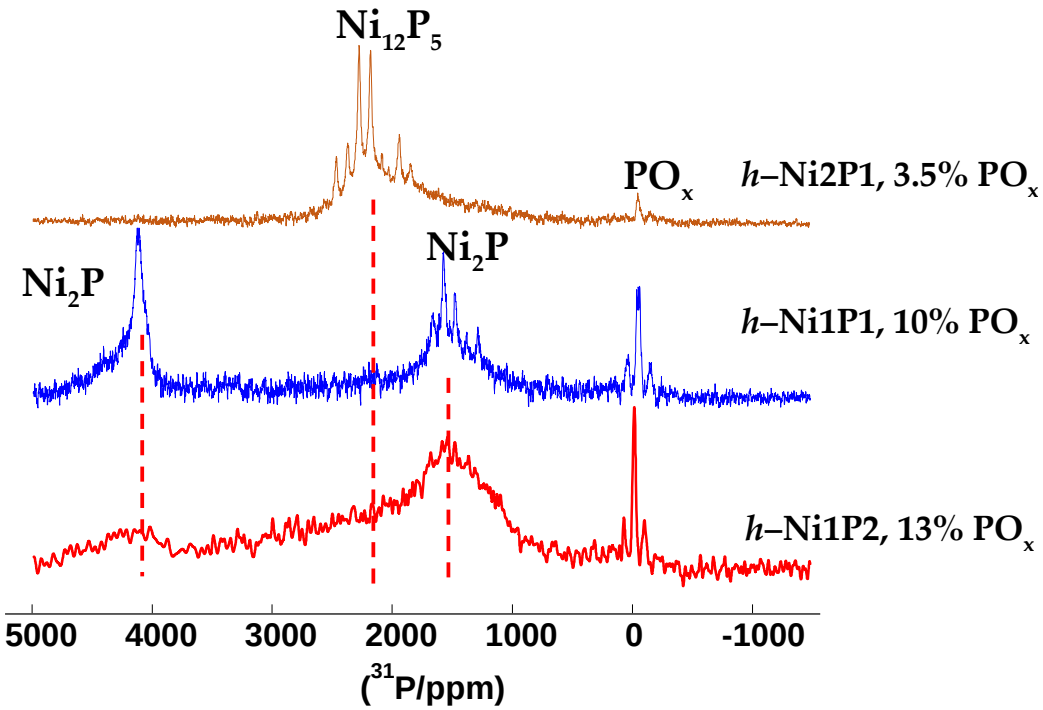

Figure 3. Spin-echo ^{31}P 14 kHz MAS NMR spectra of high-loaded Ni_xP_y/SiO_2 catalysts with different initial Ni/P molar ratio (2/1, 1/1 and 1/2 top-down) reduced at 600 °C. Spectra are normalized to the same amplitude of the highest point.

Summarizing the XRD, TEM and NMR results of catalysts characterization the several conclusions have to be indicated. XRD and ^{31}P MAS NMR data showed that the initial Ni/P molar ratio influences on phase composition of reduced phosphide catalysts: Ni_2P is produced using the initial Ni/P molar ratio of 1 and 0.5, while the initial Ni/P molar ratio of 2 favors formation of $Ni_{12}P_5$ phase in accordance with the previous results [7,8,37,38]. The TEM data showed that high-loaded samples (*h*-Ni2P1, *h*-Ni1P1, and *h*-Ni1P2) contain phosphide particles with the broad particle size distribution (from 2 to 20 nm). On the contrary, the TEM images of the low-loaded samples demonstrated uniformly distributed phosphide particles with approximately the same mean particle diameter. ^{31}P MAS NMR results let us estimate the portion of P entering in the PO_x groups on the surface of high-loaded samples, showing the enrichment of the catalysts with phosphate species as the Ni/P ratio decreases.

Unfortunately, such estimation cannot be done in the case of the low-loaded samples due to the low intensity of the ^{31}P MAS NMR signals. Previously it was stated that namely the PO_x groups are responsible for the Brønsted acidity of Ni_xP_y/SiO_2 catalysts [7,26,28,37,42,43].

The obtained set of low-loaded samples are the appropriate candidates for comparing catalytic behavior in methyl palmitate hydrodeoxygenation due to approximately the same mean particle diameters and narrow particle size distributions of the nickel phosphide on silica. At the same time, high-loaded samples provide a reliable insight into the nature of the active phase in nickel phosphide catalysts.

2.2. Catalytic Performance of Nickel and Nickel Phosphide Catalysts

2.2.1. Mass-Transfer Process in Methyl Palmitate HDO

In order to evaluate the effect of internal diffusion on catalytic HDO, the Weisz-Prater criterion was used [44]. For negligible diffusional limitations the Weisz-Prater number estimated by equations is less than 0.3:

$$N_{W-P} = \frac{A_{M.S.} \cdot R^2_{particles}}{C_S \cdot D_{eff}} \leq 0.3 \quad (1)$$

where $A_{M.S.}$ is the observed reaction rate, $R_{particles}$ is the catalyst particles radius, C_s is the reactant surface concentration and D_{eff} is the effective diffusion coefficient. The details of the procedure used for calculation of the Weisz-Prater numbers in case of methyl palmitate HDO was described previously in reference [15]. The Weisz-Prater numbers for hydrogen and methyl palmitate for the most active high-loaded *h*-Ni1P2 sample in methyl palmitate HDO were found at a temperature of 290 °C, hydrogen pressure 3.0 MPa, H_2/feed volume ratio 600 Nm^3/m^3 and LHSV of 10.7 h^{-1}. The values of $N_{W\text{-}P\ H2}$ = 0.02 and $N_{W\text{-}P\ MP}$ = 0.16 indicate the negligible internal mass transfer effects on HDO rate.

2.2.2. Catalytic Performance of Nickel Phosphide Catalysts in Methyl Palmitate HDO

Catalytic properties of nickel phosphide catalysts were investigated in the HDO of methyl palmitate (10 wt % methyl palmitate in *n*-dodecane) in a trickle-bed reactor at a temperature of 290 °C, hydrogen pressure 3.0 MPa, H_2/feed volume ratio 600 Nm^3/m^3, LHSV of methyl palmitate varied in the interval from 0.3 to 16 h^{-1}. The X_{MP}—LHSV dependencies were obtained to follow the evolution of methyl palmitate (MP), intermediates and the end products in the course of the reaction. The reaction rates normalized per gram of catalysts (A_{HDO}) and per metal sites (TOF) were calculated at the MP conversion level about 15–20% (for details see Section 3.3).

The catalytic properties of silica-supported Ni phosphide catalysts with different initial Ni/P molar ratio and Ni content are summarized in Table 2. The comparison of the rate of MP transformation (A_{HDO}) over two sets of catalysts let us see that A_{HDO} is lower over the high-loaded sample with the same Ni/P ratio. Decreasing of Ni/P molar ratio favors increasing of A_{HDO} over both high- and low-loaded samples (Figure 4). Broad particle size distributions of phosphide phases on the surfaces of high-loaded *h*-Ni2P1, *h*-Ni1P1, and *h*-Ni1P1 samples does not allow us to compare the activity of these catalysts calculated per metal site (TOF). The TOF were calculated for the samples with nearly the same size of Ni phosphide nanoparticles (*l*-Ni2P1, *l*-Ni1P1, and *l*-Ni1P2). The trend is the same as for A_{HDO}—with the decrease of Ni/P molar ratio TOF increases visibly from 5.31 s^{-1} over *l*-Ni2P1 to 10.65 s^{-1} over *l*-Ni1P1 and 14.3 s^{-1} over *l*-Ni1P2. The difference in the activities of *l*-Ni2P1 and the other samples can be explained by the difference in the active phase composition ($Ni_{12}P_5$ versus Ni_2P), but both *l*-Ni1P1 and *l*-Ni1P2 samples contain Ni_2P phase. The main difference between these two samples is the lower Ni/P ratio in the *l*-Ni1P2 samples, while the mean sizes of Ni phosphide particles are similar. In turn, the decrease of Ni/P ratio led to the of phosphate groups content on the surface of phosphide catalysts (Figure 3).

Table 2. Catalytic properties of silica-supported nickel and nickel phosphide catalysts in methyl palmitate HDO. Reaction conditions: P_{H2} = 3.0 MPa, T = 290 °C, H_2/feed = 600 Nm^3/Nm^3, LHSV = 1.5–16.0 h^{-1}.

Catalyst	Ni/P Molar Ratio in Precursor	XRD Phase	A_{HDO}, mol/(h·g $_{of\ Ni}$)	$A_{M.S.}\cdot 10^3$, s^{-1}	Sc_{16}, %
h-Ni	-	Ni	8.8×10^{-3}		12.7
h-Ni2P1	2	$Ni_{12}P_5$	3.4×10^{-2}		28.0
h-Ni1P1	1	Ni_2P	8.2×10^{-2}		28.8
h-Ni1P2	0.5	Ni_2P	1.8×10^{-1}		32.8
l-Ni2P1	2	$Ni_{12}P_5$	7.6×10^{-2}	5.31	25.8
l-Ni1P1	1	Ni_2P	1.4×10^{-1}	10.65	32.1
l-Ni1P2	0.5	Ni_2P	2.5×10^{-1}	14.33	31.5

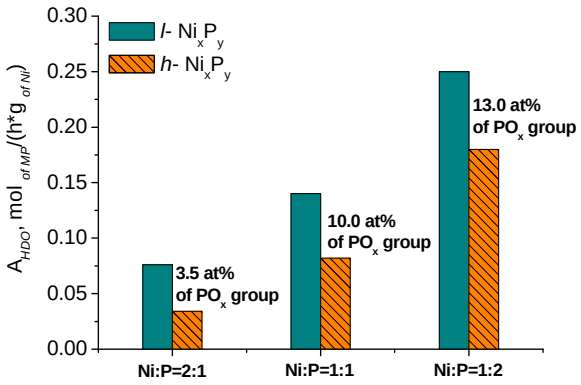

Figure 4. A_{HDO} (mol/(h·g $_{of\ Ni}$)) versus PO_x (at %) for the catalysts with different Ni/P molar ratios: Ni2P1, Ni1P1, and Ni1P2. Catalytic activity, A_{HDO}, of 2.5 wt % Ni_xP_y/SiO_2 and 7.0 wt % Ni_xP_y/SiO_2 catalysts prepared with different Ni:P molar ratios in methyl palmitate HDO at the temperature = 290 °C and hydrogen pressure = 3.0 MPa. For the series of 7.0 wt % Ni_xP_y/SiO_2 catalysts (*h*-Ni2P1, *h*-Ni1P1, and *h*-Ni1P2) it was pointed the amount of PO_x (at %) determined by ^{31}P magic angle-spinning (MAS) nuclear magnetic resonance (NMR).

So, the obtained results have shown the increase of catalytic activity of silica-supported phosphide catalysts in methyl palmitate HDO with the decrease of Ni/P ratio in the sets of catalysts with nearly the same Ni content. This trend coincides with the increase of the PO_x groups' content percentage observed by NMR in high-loaded samples with the decrease of Ni/P ratio (3.5, 10 and 13 at % of the total P content in the *h*-Ni2P1, *h*-Ni1P1, and *h*-Ni1P2). Unfortunately, the quantitative estimation of the amount of PO_x groups in the low-loaded sample is questionable because of the low intensities of the corresponding signals. But considering the similarity in the phase composition and TPR profile (see Figure S2 in Supplementary Materials) between the low- and high-loaded samples with the close Ni/P ratio, we can presume the same trend of PO_x groups' dependence on Ni/P ratio in both sets of catalysts. The evolution of catalytic activity with the Ni/P ratio can be explained by the change of the amount of PO_x surface groups, taking into account the tentative scheme of methyl palmitate conversion and the possible role of PO_x groups that is known to display Brønsted acidity in the Ni_xP_y/SiO_2 catalysts [7,26,28,37,42,43].

The tentative reaction network of MP transformation over silica-supported Ni phosphide catalysts is considered, taking into account the liquid product distribution, the gas phase analysis and the literature data concerning the HDO of fatty acid ethers [7,10,12–14]. The reaction network of methyl palmitate HDO (Figure 5) has been proposed including several types of reactions which can occur over metal (hydrogenation-dehydrogenation, hydrogenolysis of C-O and C-C bonds) and acid (hydrolysis, esterification, dehydration) active sites [14]. The analysis of product distribution

depending on LHSV shows that the main products of methyl palmitate HDO are C_{15} and C_{16} alkanes, while only minor quantities of intermediate O-containing products, namely palmitic acid, hexadecanal, hexadecanol and palmityl palmitate are detected in all the experiments regardless of the Ni content and Ni/P ratio (Figures 6–8). The formation of negligible amounts of O-containing intermediates is confirmed by a minor difference between the conversion of methyl palmitate and overall conversion of oxygen-containing compounds defined by CHNSO elemental analysis (Figure 9). These observations indicate that the oxygen-containing intermediates are transformed further immediately after their production from methyl palmitate, that is, the transformation of methyl palmitate limits of the overall HDO reaction producing C_{15} and C_{16} alkanes as the end products. As a consequence, first of all, the possible routes of methyl palmitate conversion to the intermediates should be analyzed.

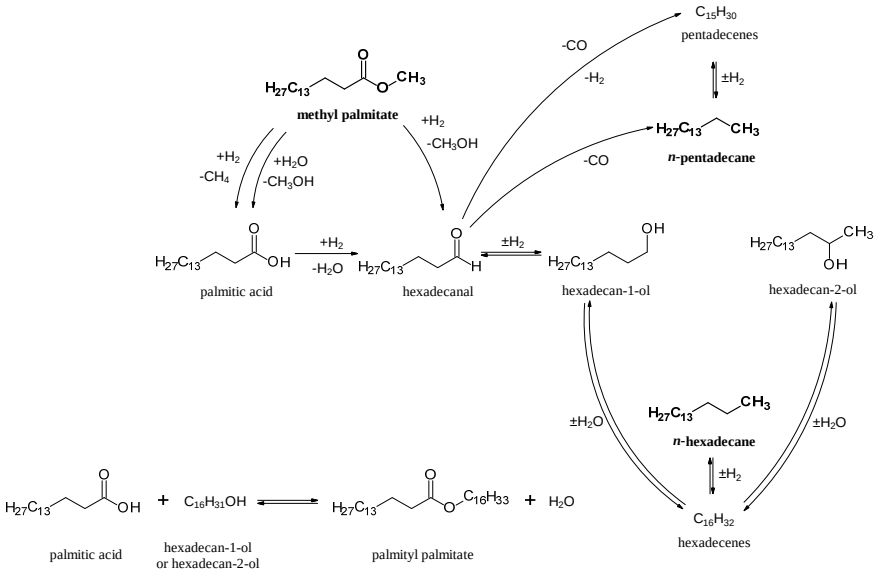

Figure 5. Proposed reaction network over silica-supported nickel phosphide catalysts.

It was proposed in many studies [2,4,7,10,13,14,45] that methyl palmitate transformation proceeds through the formation of palmitic acid or hexadecanal as a primary intermediate (Figure 5). Both possibilities exist for the production of palmitic acid in the HDO of methyl palmitate: via the hydrogenolysis of the C-O bond of ester groupover metal sites with the formation of CH_4 along with acid or through acid-catalyzed hydrolysis of ester with water leading to the formation of methanol. Hexadecanal can be formed through the direct hydrogenolysis of the C-O σ-bond of the methyl palmitate carboxylic group leading to hexadecanal and methanol: the second possible way of hexadecanal formation involves hydrogenation of palmitic acid, accompanied with the production of water. Among the listed transformation of methyl palmitate only hydrolysis requires the acid functionality, so the increase of the PO_x groups amount in the row of catalysts Ni2P1 < Ni1P1 < NiP2 the acceleration of methyl palmitate transformation due to the acid-catalyzed hydrolysis. Several research groups have already reported an increase of Brønsted acid site quantities determined by means of NH_3-TPD techniques and assigned to P-OH species with the decrease of Ni/P ratio in the silica-supported nickel phosphide catalysts [7,28,37,42,43].

In our experiments, the *h*-Ni_xP_y catalysts displayed a higher activity in methyl palmitate HDO that supported Ni/SiO_2 catalyst (D_{XRD} = 10.7 nm) with nearly the same content of nickel (Figure 10). While Ni/SiO_2 catalyst produces pentadecane with the selectivity about 90% in all range of the experiments, SiO_2 and PO_x/SiO_2 produce only palmitic acid as a result of acid-catalyzed hydrolysis of MP. Additional amount of dodecanol causes the decrease of the rate of MP transformation when HDO of MP and dodecanol mixture was performed over the *l*-Ni1P2 catalyst (see Figure S3 in Supplementary Materials), pointing out to the competition of dodecanol with the MP molecules

for the acid sites and testifying the participation of these sites in the MP conversion. The above observations confirm implicitly the important role of acid sites in the methyl palmitate transformation to the intermediates. The analysis of products distribution in the gas phase provides additional information about possible reaction routes of MP and oxygen-containing intermediates transformation. Among the gas phase products of methyl palmitate HDO methane, CO and some amounts of methanol were observed. The absence of CO_2 in the outlet gas indicates that palmitic acid does not produce the C_{15} hydrocarbons through the decarboxylation ($DeCO_2$) route. Further conversion of acid most probably proceeds through the hydrogenation to hexadecanal which in turn gives *n*-pentadecane and *n*-pentadecene through decarbonylation reaction or hexadecanol through hydrogenation reaction. The latter is the main source of C_{16} paraffin via elimination of water from hexadecanol with the formation of hexadecene and subsequent hydrogenation of hexadecene to *n*-hexadecane [15]. Obtained data on selectivity in methyl palmitate HDO correlate well with gas phase data: CO concentration in the gas phase is proportional to n-pentadecane content in the liquid products (see Figure S4 in Supplementary Materials). Authors [7,12,14] reported decarbonylation of methyl laurate (with the formation of undecene) or lauric acid (producing undecanol) but we do not have any evidence that these reactions take place. Moreover, the decarbonylation of palmitic acid should produce alcohol with 15 carbon atoms, but oxygen-containing compounds with 15 carbon atoms in hydrocarbon chain were not detected. Instead, pentadecene was found among the reaction products in small amounts, pointing out to the possibility of hexadecanal decarbonylation producing pentadecene and pentadecane (Figure 5). So, the observed peculiarities make hexadecanal the most probable source of C_{15} hydrocarbons.

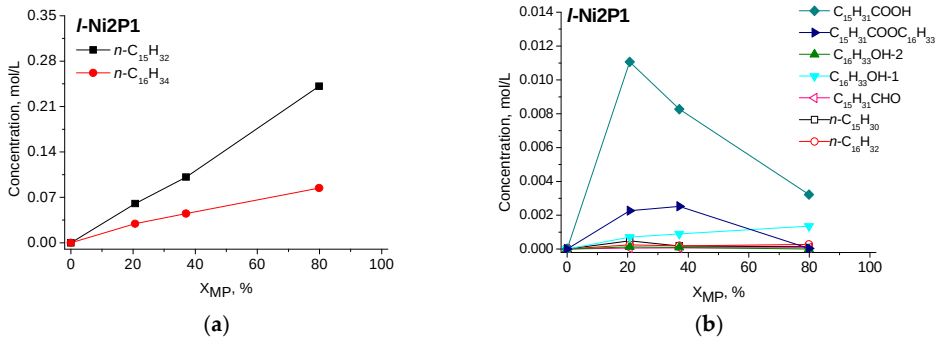

Figure 6. Concentration profiles of liquid-phase components during methyl palmitate HDO over *l*-Ni2P1 catalyst: (**a**) the main products—C_{15} and C_{16} hydrocarbons; (**b**) the observed intermediates. Reaction conditions: P_{H2} = 3.0 MPa, T = 290 °C, H_2/feed = 600 Nm^3/Nm^3, LHSV = 0.3–1.5 h^{-1}.

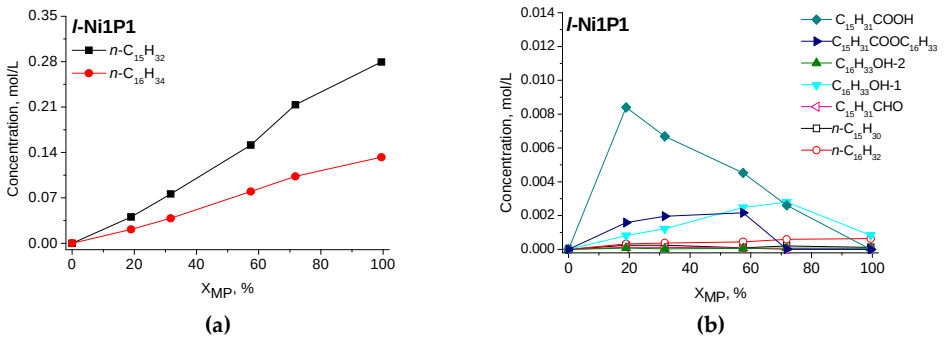

Figure 7. Concentration profiles of the liquid-phase components during methyl palmitate HDO over *l*-Ni1P1 catalyst: (**a**) the main products—C_{15} and C_{16} hydrocarbons; (**b**) the observed intermediates. Reaction conditions: P_{H2} = 3.0 MPa, T = 290 °C, H_2/feed = 600 Nm^3/Nm^3, LHSV = 0.3–3.2 h^{-1}.

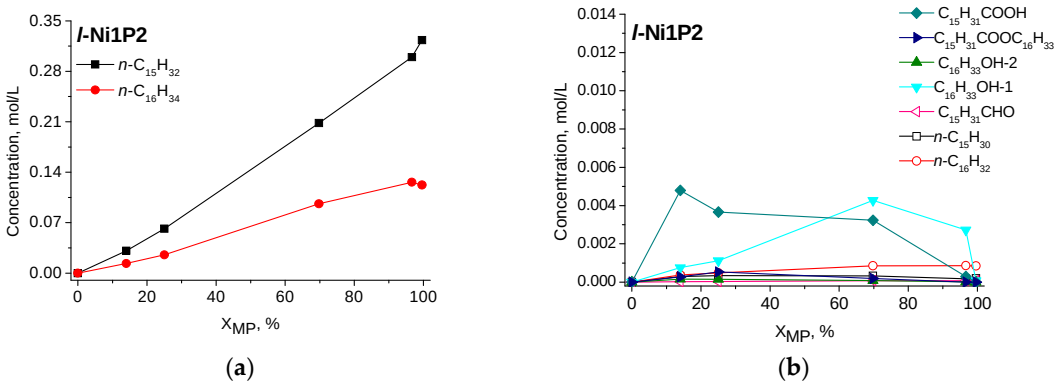

Figure 8. Concentration profiles of the liquid-phase components during methyl palmitate HDO over *l*-Ni1P2 catalyst: (**a**) the main products—C_{15} and C_{16} hydrocarbons; (**b**) the observed intermediates. Reaction conditions: P_{H2} = 3.0 MPa, T = 290 °C, H_2/feed = 600 Nm^3/Nm^3, LHSV = 0.3–6.4 h^{-1}.

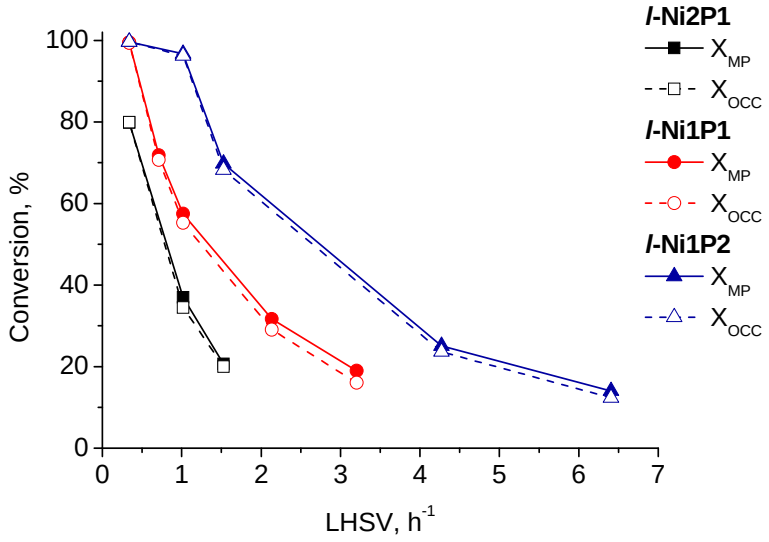

Figure 9. Methyl palmitate (X_{MP}) and oxygen (X_{OCC}) conversions versus liquid hourly space velocity (LHSV) of MP (h^{-1}) over the low-loaded nickel phosphide catalysts with different Ni/P molar ratios: *l*-Ni2P1, *l*-Ni1P1 and *l*-Ni1P2. Reaction conditions: P_{H2} = 3.0 MPa, T = 290 °C, H_2/feed = 600 Nm^3/Nm^3, LHSV = 0.3–6.4 h^{-1}.

To clarify the routes of acid transformation the additional experiments were done using lauric acid as a model compound. Just only CO was observed in the exhaust gas of lauric acid HDO over the *l*-Ni1P2 catalyst, wherein CO does not give methane at least up to 360 °C (Figure 11). So, methane observed among the product of methyl palmitate HDO can be produced through the methyl palmitate hydrogenolysis or as a result of methanol hydrogenation. The choice between these two contributions is rather complicated since the quantitative analysis of methanol is failed due to its hydrophilicity causing the agglomeration of methanol with the produced water.

Selectivity of methyl palmitate conversion to C_{15} and C_{16} hydrocarbon (at overall oxygen conversion of 100%) does not display the evident dependence on the Ni/P ratio (Table 2), indicating the minor effect of the phosphate groups on the C_{16}/C_{15} selectivity. The most active *h*-Ni1P2 catalysts demonstrated stable behavior in the time-on-stream experiments at least for 15 h (see Figure S5 in Supplementary Materials).

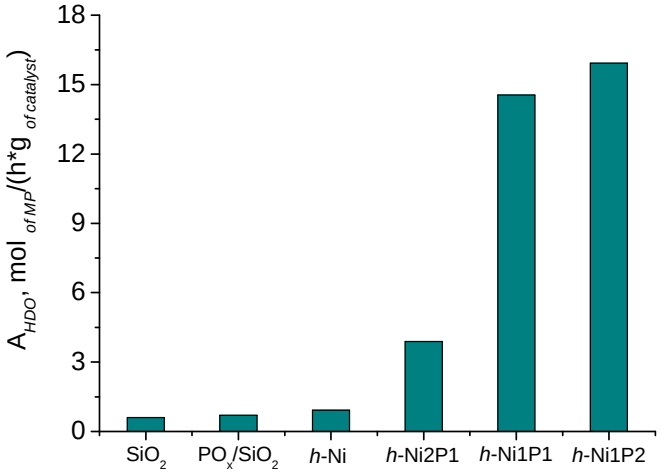

Figure 10. Evolution of the A_{HDO} (mol $_{of\ MP}$/h·g $_{of\ catalyst}$) with the nature of the catalyst: *h*-Ni, *h*-Ni2P1, *h*-Ni1P1, *h*-Ni1P2 and the reference samples SiO_2 and PO_x/SiO_2. Reaction conditions: P_{H2} = 3.0 MPa, T = 290 °C, H_2/feed = 600 Nm^3/Nm^3, LHSV = 0.3–6.4 h^{-1}.

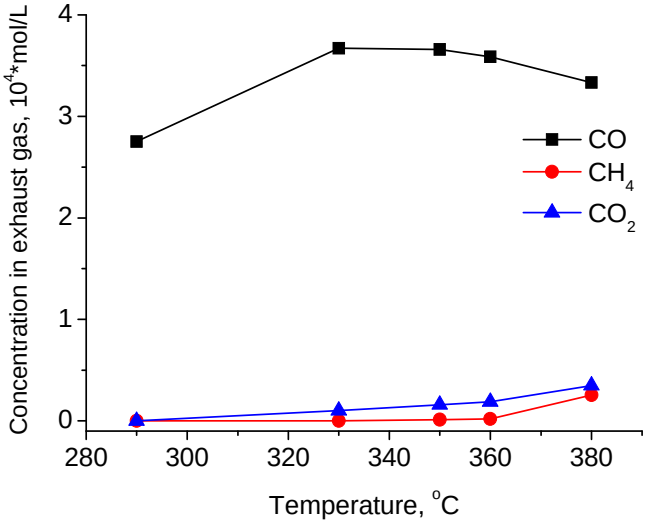

Figure 11. Temperature dependence of the exhaust gas composition during lauric acid HDO over *l*-Ni1P2 catalyst. Reaction conditions: feed composition 7.41 wt % lauric acid in *n*-octane, P_{H2} = 3.0 MPa, T = 290—380 °C, H_2/feed = 600 Nm^3/Nm^3, LHSV = 2.16 h^{-1}.

3. Materials and Methods

3.1. Catalyst Preparation

Commercial spherical silica «KSKG» (Salavat, Russia, pore volume—0.80 cm^3/g, average pore diameter—10.6 nm) was purchased from «ChromAnalit» Ltd. (Moscow, Russia) and has been used as a support. Prior to use, the silica was dried at 110 °C for 7 h and calcined at 500 °C for 4 h. Afterwards, it was crushed and sieved to 0.25–0.50 mm.

Ni_xP_y/SiO_2 catalysts synthesis. The silica-supported nickel phosphide catalysts were prepared by temperature-programmed reduction (TPR) of nickel- and phosphate-containing precursors, with varying initial Ni/P molar ratio, namely 2/1, 1/1 and 1/2 (samples were denoted as Ni2P1, Ni1P1, and Ni1P2, correspondingly). The optimal reduction conditions for the Ni_2P/SiO_2 catalysts prepared from the nickel phosphate precursors were chosen according to the earlier results [15] and were stated to 600 °C for 1 h The initial amount of nickel precursor in the impregnated solution for synthesized

catalyst was 2.1×10^{-3} mol of Ni per gram of support for high-loaded samples (denoted as *h* series) or 5.2×10^{-4} mol of Ni per gram of support for low-loaded samples (denoted as *l* series). The procedure for catalyst preparation follows: silica (0.25–0.50 mm) was incipiently impregnated with an aqueous solution of $Ni(CH_3COO)_2 \cdot 4H_2O$ («Reakhim», Samara, Russia, 99.5%) and $(NH_4)_2HPO_4$ («Alfa Aesar», Ward Hill, MA, USA, technical grade, $P_2O_5 \leq 53$ wt %) stabilized by nitric acid («Reakhim», Samara, Russia, 70 wt %). The impregnated sample was dried at 110 °C for 4 h and calcined at 500 °C for 4 h. The obtained oxide precursor was reduced in hydrogen (flow rate = 150 mL/min per gram of precursor) at 600 °C (ramp = 1 °C/min) for 1 h and then cooled to room temperature. Finally, the sample was passivated in 1% O_2/He flow (flow rate = 80 mL/min) for 2 h at room temperature.

Ni/SiO_2 catalyst synthesis. The reference Ni/SiO_2 catalyst (*h-Ni*) was prepared by incipient wetness impregnating of silica granules with an aqueous solution of $Ni(CH_3COO)_2 \cdot 4H_2O$ containing 2.1×10^{-3} mol of Ni per gram of support, followed by drying at 110 °C for 4 h and then calcined at 500 °C for 4 h. The precursor was reduced by TPR in H_2 flow (flow rate = 60 mL/min) at 400 °C (ramp = 1 °C/min) for 4 h to obtain Ni/SiO_2 catalyst. Finally, the sample was passivated in 1% O_2/He flow (flow rate = 80 mL/min) for 2 h at room temperature.

The PO_x/SiO_2 (h-P_{ox}) reference sample was prepared by impregnating of silica with an aqueous solution of $(NH_4)_2HPO_4$ (4.2×10^{-3} mol of P per gram of support), followed by drying at 110 °C for 4 h and calcination at 500 °C for 4 h Prior to use in hydrodeoxygenation, the precursor was activated by standard TPR procedure by heating in H_2 flow at 600 °C for 1 h.

3.2. Catalyst Characterization

The elemental analysis of the catalysts was performed using inductively coupled plasma atomic emission spectroscopy (ICP-AES) on Optima 4300 DV (Perkin Elmer, Villebon-sur-Yvette, France).

The textural properties of the catalysts were determined using nitrogen physisorption at 77 K with an ASAP 2400 instrument (USA).

XRD measurements were performed on an X-ray diffractometer Bruker D8 Advance (Bruker, Karlsruhe, Germany) using CuK_α radiation (wavelength λ = 1.5418 Å) in the 2θ scanning range of 10°–70°. The qualitative phase analysis was carried out using the JCPDS data base [46]. The quantitative phase analysis and refining of the unit cell parameters were carried out by Rietveld analysis of a diffraction pattern using X'Pert High Score Plus software. The average crystallite size (D_{XRD}) was calculated using the Scherrer equation applied to the (312) reflection at 2θ = 48.9° of $Ni_{12}P_5$ phase and to the (111) reflection at 2θ = 40.6° of Ni_2Pphase correspondingly. The average crystallite size (D_{XRD}) of $Ni_{12}P_5$ nanoparticles was calculated using the Scherrer equation applied to the (312) reflection at 2θ = 48.9°.

The samples were investigated using high-resolution transmission electron microscopy with a JEM-2010 transmission electron microscope (JEOL, Tokyo, Japan) with accelerating voltage of 200 kV and resolution of 0.14 nm. The local elemental composition was analyzed with an energy-dispersive EDX spectrometer equipped with a Si(Li) detector (energy resolution—130 eV). To obtain statistical information, the structural parameters of ca. 500 particles were measured. To determine the mean particles diameter (D_s), the Sauter mean diameter was used calculated by the equation:

$$D_S = \frac{\sum n_i d_i^3}{\sum n_i d_i^2} \quad (2)$$

where n_i is the number of particles, d_i is the diameter of the *i*th particle.

The samples of the catalyst precursors were characterized by the H_2 temperature-programmed reduction method (H_2-TPR). An amount of 0.10 g of the calcined sample was loaded into a quartz U-tube reactor (inner diameter equal to 4 nm). The experiments were carried out in 10 vol % H_2/Ar flow (flow rate = 60 mL/min) at heating rate 10 °C/min in a temperature region from 80 to 900 °C.

The H_2 consumption was determined by a thermal conductivity detector (TCD). A cold trap (−60 °C) before the TCD was used in order to remove water from exhaust gas.

NMR experiments were carried out using a Bruker Avance-400 spectrometer at the resonance frequency of 161.923 MHz for ^{31}P. Magic Angle Spinning (MAS) spectra were measured using a Bruker MAS NMR probe with 4-mm (outer diameter) ZrO_2 rotors at spinning frequency of 14 kHz. The ^{31}P spectra were obtained using Hahn-echo sequence using a train of $\pi/2$-τ-π pulses, the duration of $\pi/2$ was 2.4 μs. The interpulse delay τ was chosen with respect to the rotation frequency. The sequence repetition delay was 100 ms due to very short ^{31}P relaxation time in Ni-P intermetallic compounds [47]. Due to very large spectra width, all spectra were collected by frequency stepped technique with a step of 600 ppm (with respect to ^{31}P NMR frequency, ~100 kHz) covering ~5000–6000 ppm spectral width, the details can be found elsewhere [48]. The spectra were collected at room temperature and referenced to 85% water solution of orthophosphoric acid (for ^{31}P experiments). The accuracy of the chemical shift was ±0.5 ppm. The number of transients was 16k in each frequency point. To avoid reduced catalyst oxidation by air, all samples were sealed in glass ampoules without oxygen access. Prior to NMR experiments, the catalysts were transferred from ampoule to NMR rotor in a glove box under argon atmosphere. This technique helps to minimize possible oxidation during NMR spectra acquisition.

3.3. Experimental Setup and Procedure

Methyl palmitate («Sigma-Aldrich», St. Louis, MO, USA, grade ≥ 97%), lauric acid («Sigma-Aldrich», St. Louis, MO, USA, grade ≥ 98%), dodecanol-1 («Sigma-Aldrich», St. Louis, MO, USA, grade ≥ 98%), *n*-dodecane («Acros Organics», New Jersey, USA, grade ≥ 99%) and *n*-octane («Kriokhrom», Saint Peterburg, Russia, grade ≥ 99.5%) were used for initial reaction mixtures preparation.

The catalytic activity in HDO of the methyl palmitate was evaluated in the trickle-bed reactor (inner diameter 9 mm and total length 265 mm) at the temperature 290 °C, hydrogen pressure 3.0 MPa, H_2/feed volume ratio 600 Nm^3/Nm^3, LHSV of MP was varied from 0.3 to 16 h^{-1}. The composition of the reaction mixture, wt %: methyl palmitate—10 (oxygen content—1.183 wt %), *n*-octane (used as an internal standard for quantification of liquid product)—2 and the rest—*n*-dodecane. The catalyst was placed in the middle part of the reactor between two layers of silicon carbide—inert material with high thermal conductivity, a layer of fine particles of catalyst diluted (0.2 ÷ 0.3 mm) silicon carbide in a ratio 1:4 to improve the wettability and uniformity of the liquid distribution in the catalyst layer, minimizing the effect of the wall surface and axial flow heterogeneity. Prior to the reaction, the passivated catalyst was re-reduced in situ in hydrogen (flow rate = 60 ml/min) at 400 °C and hydrogen pressure 5.0 MPa for 15 h. The liquid products were collected every hour till steady-state condition, and time on stream was not less than 8 h.

The conversion of methyl palmitate (X_{MP}), conversion of oxygen-containing compounds (X_{OCC}) and the selectivity to C_{16} hydrocarbons (S_{C16}) were calculated as follows:

$$X_{MP} = \left(1 - \frac{n_{MP}}{n^o_{MP}}\right) \times 100, \% \quad (3)$$

$$X_{OCC} = \left(1 - \frac{n_O}{n^o_O}\right) \times 100, \% \quad (4)$$

$$S_{C16} = \left(\frac{n_{C16}}{n^o_{MP} - n_{MP}}\right) \times 100, \% \quad (5)$$

where n°_{MP} and n_{MP} are the initial and the current methyl palmitate content in the reaction mixture expressed in mols, n°_O and n_O are the initial and current oxygen content in the reaction mixture expressed in mols, n_{C16} is the amount of C_{16} hydrocarbons in the products at X_{MP} = 100% expressed in mols.

The apparent catalytic activity (A_{HDO}) of the samples in methyl palmitate HDO was evaluated as follows:

$$A_{HDO} = \frac{X_{OCC} \cdot F}{\omega_{cat} \cdot C_{Ni}}, \frac{mol}{g \cdot h} \quad (6)$$

where X_{OCC} is the conversion of oxygen-containing compounds (%), F is the molar rate of methyl palmitate fed into the reactor (mol·h^{-1}), ω_{cat} is the catalyst weight (g) and C_{Ni} is the nickel content in the catalyst (wt %). A_{HDO} was calculated at the MP conversion below 20%.

The HDO activity (TOF.) of the samples per metal site was estimated by the equation:

$$TOF = \frac{X_{MP} \cdot F}{\omega_{cat} \cdot C_{M.S.}}, \frac{1}{s} \quad (7)$$

where X_{MP} is the conversion of methyl palmitate (%), F is the molar rate of methyl palmitate (mol·s^{-1}), ω_{cat} is the catalyst weight (g) and $C_{M.S.}$ is the theoretical metal site concentration [49] (mol·g^{-1}) calculated assuming cubic or spherical geometry of nickel phosphide particles uniformly distributed on the surface as follows:

$$C_{M.S.} = \frac{6 \cdot \eta \cdot C_{Ni_xP_y}}{\rho_{Ni_xP_y} \cdot D_S}, \frac{mol}{g} \quad (8)$$

in which η is surface metal atom density, ρ_{NixPy} is the bulk density of Ni_xP_y phase (Table 3) and D_S is the Sauter mean particles diameter obtained from TEM measurements, C_{NixPy} is the fractional weight loading of nickel phosphide in the catalyst ($\omega_{NixPy}/\omega_{cat}$). The theoretical metal atom site concentration is an approximate parameter.

Table 3. Surface metal density and bulk density of nickel and nickel phosphide.

Compound	Surface Metal Density, η (Atoms·cm^{-2})	Compound Density, ρ (g·cm^{-3})
Ni_2P	1.01×10^{15} [49]	7.35 [50]
$Ni_{12}P_5$	1.21×10^{15}	7.53 [50]

3.4. Products Analysis

The reaction products were identified using a GC/MS technique (Agilent Technologies 7000 GC/MS Triple QQQ GC System 7890A, Santa Clara, CA, USA) with a VF-5MS quartz capillary column (30 m × 0.25 mm × 0.25 µm). The liquid samples were analyzed with a gas chromatography system (Agilent 6890N, Santa Clara, CA, USA) equipped with HP-1MS column (30 m × 0.32 mm × 1.0 µm) and flame ionization detector (FID). Gaseous phase products were analyzed online with a gas chromatograph (Chromos 1000, Dzerzhinsk, Russia) equipped with a column packed with 80/100 mesh HayeSep® (Sigma-Aldrich, St. Louis, MO, USA) and FID. The concentrations of CO and CO_2 were analyzed in the form of methane after methanation over reduced Pd catalyst at 340 °C. The carbon balance across the reactor for all experiments was >95%.

The total oxygen content in the reaction mixture was determined using CHNSO elemental analyzer Vario EL Cube (Elementar Analysensysteme GmbH, Hanau, Germany).

4. Conclusions

To get a deeper insight into the Ni/P effect on the catalytic properties of silica-supported nickel phosphide catalyst in the aliphatic ester HDO two sets of the Ni_xP_y/SiO_2 catalysts differing in nickel content were prepared. Both high-loaded and low-loaded set of catalysts contain the samples with the initial Ni/P ratios adjusted to 2/1, 1/1 and 1/2. Set of high-loaded samples (*h*-Ni_xP_y/SiO_2) provides a reliable insight into the evolution of the active phase with the Ni/P decrease, while the set of low-loaded samples (*l*-Ni_xP_y/SiO_2) is an appropriate candidate for comparing catalytic behavior

in the terms of TOF due to the similar value of the mean particle sizes in the catalysts with different Ni/P values.

Summarizing the XRD, TEM and NMR results of catalysts characterization it was concluded that the initial Ni/P molar ratio influences phase composition of the reduced phosphide catalysts: Ni_2P produced using the initial Ni/P molar ratio of 1 and 0.5, while the initial Ni/P molar ratio of 2 favors formation of $Ni_{12}P_5$ phase. According to TEM data have shown the high-loaded samples (*h*-Ni2P1, *h*-Ni1P1, and *h*-Ni1P2) was shown with TEM contain phosphide particles with the broad particle size distribution (from 2 to 20 nm), while uniformly distributed phosphide particles with the mean particle diameter 4.9 nm for *l*-Ni2P1), 4.7 nm for *l*-Ni1P1 and 3.5 nm for *l*-Ni1P2 were observed. ^{31}P MAS NMR results showed that an increase of Ni/P ratio is accompanied by the increase of the PO_x groups on the surface of high-loaded samples; the same dependence was speculated for the low-loading samples taking into account the similarities in the active phase composition and TPR behavior.

Catalytic activity in methyl palmitate HDO normalized to metal content was found to increase with the decrease of Ni/P content in the catalysts and such dependence was true for both sets of catalysts. The same trend of TOF increase over the *l*-Ni_xP_y/SiO_2 catalysts was explained by the acceleration of methyl palmitate transformation due to the hydrolysis of methyl palmitate over acid PO_x groups of the nickel phosphide catalysts. The obtained dependence corroborates our previous results, where the increase of phosphate groups content through the adjusting of phosphorus precursor and reduction temperature provides the increase of methyl palmitate conversion rate in HDO [15].

The decrease of Ni/P ratio in the silica-supported nickel phosphide catalysts was shown to increase the rate of methyl palmitate conversion most probably through the hydrolysis of methyl palmitate over acid sites presented by the phosphate groups of the silica-supported nickel phosphide catalysts. Thus, the employment of support with the pronounced acidity for the preparation of supported phosphide catalysts can significantly increase the rate of fatty ether HDO and alkane production. However, the appropriate balance of acid and metal functionalities is crucial to provide the high catalytic activity of phosphide catalysts in the overall reaction of methyl palmitate HDO, comprising the variety of acid-catalyzed and metal-catalyzed reactions.

Supplementary Materials: The following are available online at www.mdpi.com/2073-4344/7/10/298/s1. Figure S1: TEM images of Ni_xP_y/SiO_2 catalysts with different initial molar Ni/P ratio: (a) *l*-Ni2P1; (b) *l*-Ni1P1; (c) *l*-Ni1P2, Figure S2: H_2-TPR profiles of Ni_xP_y/SiO_2 catalyst oxide precursors with different nickel phosphide loading: *h*-Ni1P2 and *l*-Ni1P2, Figure S3: Effect of the dodecanol additive on methyl palmitate conversion during HDO over *l*-Ni1P2 catalyst. Feed composition: mixture 1–10.0 wt % MP in *n*-octane; mixture 2–10.0 wt % MP and 5 wt % $C_{12}H_{25}OH$ in *n*-octane. Reaction conditions: P_{H2} = 3.0 MPa, T = 290 °C, H_2/feed = 600 Nm^3/Nm^3, LHSV $_{of\ MP}$ = 1.02 h^{-1}, Figure S4: *n*-Pentadecane concentration in liquid phase versus CO concentration in exhaust gas phase during palmitic acid HDO over *l*-Ni1P2 catalyst. Reaction conditions: feed composition 5.0 wt % palmitic acid in *n*-dodecane, P_{H2} = 3.0 MPa, T = 290 °C, H_2/feed = 600 Nm^3/Nm^3, LHSV = 0.3-6.4 h^{-1}, Figure S5: Methyl palmitate and oxygen-containing compounds conversions and C_{16} hydrocarbons selectivity (S_{C16}) during methyl palmitate HDO over *h*-Ni1P2 catalysts. Reaction conditions: P_{H2} = 3.0 MPa, T = 290 °C, H_2/feed = 600 Nm^3/Nm^3, LHSV = 10.7 h^{-1}.

Acknowledgments: This work was conducted within the framework of budget project No. 0303-2016-0012 for Boreskov Institute of Catalysis. The authors are grateful to V.A. Rogov for catalysts characterization by H_2-TPR, and to V.A. Utkin and M.V. Shashkov for reaction products identification using GC/MS technique.

Author Contributions: G.A.B. conceived and designed the experiments and supervised the work; I.V.S. performed the catalyst synthesis; I.V.D., I.V.S. and P.V.A. performed the catalytic activity tests; E.Y.G. performed the catalyst characterization by TEM; V.P.P. performed the catalyst characterization by XRD; I.V.Y. and O.B.L. performed the catalyst characterization by MAS NMR; I.V.D., P.V.A., I.V.S. and G.A.B. analyzed the experimental data and wrote the paper.

Conflicts of Interest: The authors declare no conflict of interest.

References

1. Kubicka, D.; Tukac, V. Chapter 3. Hydrotreating of Triglyceride Based Feedstocks in Refineries. In *Advances in Chemical Engineering, Chemical Engineering for Renewables Conversion*, 1st ed.; Murzin, D.Y., Ed.; Academic Press: Cambridge, MA, USA, 2013; Volume 42, pp. 141–194.
2. Senol, O.I.; Viljava, T.R.; Krause, A.O.I. Hydrodeoxygenation of methyl esters on sulphided NiMo/gamma-Al_2O_3 and CoMo/gamma-Al_2O_3 catalysts. *Catal. Today* **2005**, *100*, 331–335. [CrossRef]
3. Donnis, B.; Egeberg, R.G.; Blom, P.; Knudsen, K.G. Hydroprocessing of Bio-Oils and Oxygenates to Hydrocarbons. Understanding the Reaction Routes. *Top. Catal.* **2009**, *52*, 229–240. [CrossRef]
4. Deliy, I.V.; Vlasova, E.N.; Nuzhdin, A.L.; Gerasimov, E.Yu.; Bukhtiyarova, G.A. Hydrodeoxygenation of methyl palmitate over sulfided Mo/Al_2O_3, CoMo/Al_2O_3 and NiMo/Al_2O_3 catalysts. *RSC Adv.* **2014**, *4*, 2242–2250. [CrossRef]
5. Liu, S.Y.; Zhu, Q.Q.; Guan, Q.X.; He, L.N.; Li, W. Bio-aviation fuel production from hydroprocessing castor oil promoted by the nickel-based bifunctional catalysts. *Bioresour. Technol.* **2015**, *183*, 93–100. [CrossRef] [PubMed]
6. Kordulis, C.; Bourikas, K.; Gousi, M.; Kordouli, E.; Lycourghiotis, A. Development of nickel based catalysts for the transformation of natural triglycerides and related compounds into green diesel: A critical review. *Appl. Catal. B Environ.* **2016**, *181*, 156–196. [CrossRef]
7. Chen, J.X.; Shi, H.; Li, L.; Li, K.L. Deoxygenation of methyl laurate as a model compound to hydrocarbons on transition metal phosphide catalysts. *Appl. Catal. B Environ.* **2014**, *144*, 870–884. [CrossRef]
8. Yang, Y.X.; Ochoa-Hernandez, C.; Pizarro, P.; O'Shea, V.A.D.; Coronado, J.M.; Serrano, D.P. Influence of the Ni/P ratio and metal loading on the performance of Ni_xP_y/SBA-15 catalysts for the hydrodeoxygenation of methyl oleate. *Fuel* **2015**, *144*, 60–70. [CrossRef]
9. Yang, Y.X.; Ochoa-Hernandez, C.; O'Shea, V.A.D.; Coronado, J.M.; Serrano, D.P. Ni_2P/SBA-15 As a Hydrodeoxygenation Catalyst with Enhanced Selectivity for the Conversion of Methyl Oleate Into n-Octadecane. *ACS Catal.* **2012**, *2*, 592–598. [CrossRef]
10. Guan, Q.X.; Han, F.; Li, W. Catalytic performance and deoxygenation path of methyl palmitate on Ni_2P/SiO_2 synthesized using the thermal decomposition of nickel hypophosphite. *RSC Adv.* **2016**, *6*, 31308–31315. [CrossRef]
11. Xue, Y.A.; Guan, Q.X.; Li, W. Synthesis of bulk and supported nickel phosphide using microwave radiation for hydrodeoxygenation of methyl palmitate. *RSC Adv.* **2015**, *5*, 53623–53628. [CrossRef]
12. Shi, H.; Chen, J.X.; Yang, Y.; Tian, S.S. Catalytic deoxygenation of methyl laurate as a model compound to hydrocarbons on nickel phosphide catalysts: Remarkable support effect. *Fuel Process. Technol.* **2014**, *118*, 161–170. [CrossRef]
13. Guan, Q.X.; Wan, F.F.; Han, F.; Liu, Z.H.; Li, W. Hydrodeoxygenation of methyl palmitate over MCM-41 supported nickel phosphide catalysts. *Catal. Today* **2016**, *259*, 467–473. [CrossRef]
14. Yang, Y.; Chen, J.X.; Shi, H. Deoxygenation of Methyl Laurate as a Model Compound to Hydrocarbons on Ni_2P/SiO_2, Ni_2P/MCM-41, and Ni_2P/SBA-15 Catalysts with Different Dispersions. *Energy Fuels* **2013**, *27*, 3400–3409. [CrossRef]
15. Shamanaev, I.V.; Deliy, I.V.; Aleksandrov, P.V.; Gerasimov, E.Yu.; Pakharukova, V.P.; Kodenev, E.G.; Ayupov, A.B.; Andreev, A.S.; Lapina, O.B.; Bukhtiyarova, G.A. Effect of precursor on the catalytic properties of Ni_2P/SiO_2 in methyl palmitate hydrodeoxygenation. *RSC Adv.* **2016**, *6*, 30372–30383. [CrossRef]
16. Shamanaev, I.V.; Deliy, I.V.; Pakharukova, V.P.; Gerasimov, E.Yu.; Rogov, V.A.; Bukhtiyarova, G.A. Effect of the preparation conditions on the physicochemical and catalytic properties of Ni_2P/SiO_2 catalysts. *Russ. Chem. Bull. Int. Ed.* **2015**, *64*, 2361–2370. [CrossRef]
17. Liu, Y.H.; Yao, L.; Xin, H.; Wang, G.S.; Li, D.; Hu, C.W. The production of diesel-like hydrocarbons from palmitic acid over HZSM-22 supported nickel phosphide catalysts. *Appl. Catal. B Environ.* **2015**, *174*, 504–514. [CrossRef]
18. Zarchin, R.; Rabaev, M.; Vidruk-Nehemya, R.; Landau, M.V.; Herskowitz, M. Hydroprocessing of soybean oil on nickel-phosphide supported catalysts. *Fuel* **2015**, *139*, 684–691. [CrossRef]
19. Lee, S.I.; Jeon, H.J.; Ju, S.J.; Ryu, J.W.; Oh, S.H.; Koh, J.H. Metal Phosphorus Compound for Preparing Biodiesel and Method Preparing Biodiesel Using the Same. Patent US2014/0150332A1, 5 June 2014.

20. Zhao, S.; Zhang, Z.N.; Zhu, K.Y.; Chen, J.X. Hydroconversion of methyl laurate on bifunctional Ni_2P/AlMCM-41 catalyst prepared via in situ phosphorization using triphenylphosphine. *Appl. Surf. Sci.* **2017**, *404*, 388–397. [CrossRef]
21. Zhang, Z.N.; Tang, M.X.; Chen, J.X. Effects of P/Ni ratio and Ni content on performance of gamma-Al_2O_3-supported nickel phosphides for deoxygenation of methyl laurate to hydrocarbons. *Appl. Surf. Sci.* **2016**, *360*, 353–364. [CrossRef]
22. Oyama, S.T.; Gott, T.; Zhao, H.Y.; Lee, Y.K. Transition metal phosphide hydroprocessing catalysts: A review. *Catal. Today* **2009**, *143*, 94–107. [CrossRef]
23. Sun, F.X.; Wu, W.C.; Wu, Z.L.; Guo, J.; Wei, Z.B.; Yang, Y.X.; Jiang, Z.X.; Tian, F.P.; Li, C. Dibenzothiophene hydrodesulfurization activity and surface sites of silica-supported MoP, Ni_2P, and Ni-Mo-P catalysts. *J. Catal.* **2004**, *228*, 298–310. [CrossRef]
24. Bui, P.; Cecilia, J.A.; Oyama, S.T.; Takagaki, A.; Infantes-Molina, A.; Zhao, H.Y.; Li, D.; Rodriguez-Castellon, E.; Lopez, A.J. Studies of the synthesis of transition metal phosphides and their activity in the hydrodeoxygenation of a biofuel model compound. *J. Catal.* **2012**, *294*, 184–198. [CrossRef]
25. Rodriguez, J.A.; Vines, F.; Liu, P.; Illas, F. Chapter 6. Role of C and P Sites on the Chemical Activity of Metal Carbides and Phosphides: From Clusters to Single-Crystal Surfaces. In *Model Systems in Catalysis: Single Crystals to Supported Enzyme Mimics*; Rioux, R.M., Ed.; Springer Science + Business Media: New York, NY, USA, 2010; pp. 117–132.
26. Lee, Y.K.; Oyama, S.T. Bifunctional nature of a SiO_2-supported Ni_2P catalyst for hydrotreating: EXAFS and FTIR studies. *J. Catal.* **2006**, *239*, 376–389. [CrossRef]
27. Chen, J.X.; Guo, T.; Li, K.L.; Sun, L.M. A facile approach to enhancing activity of Ni_2P/SiO_2 catalyst for hydrodechlorination of chlorobenzene: Promoting effect of water and oxygen. *Catal. Sci. Technol.* **2015**, *5*, 2670–2680. [CrossRef]
28. Abu, I.I.; Smith, K.J. The effect of cobalt addition to bulk MoP and Ni_2P catalysts for the hydrodesulfurization of 4,6-dimethyldibenzothiophene. *J. Catal.* **2006**, *241*, 356–366. [CrossRef]
29. Stinner, C.; Tang, Z.; Haouas, M.; Weber, T.; Prins, R. Preparation and ^{31}P NMR characterization of nickel phosphides on silica. *J. Catal.* **2002**, *208*, 456–466. [CrossRef]
30. Sawhill, S.J.; Layman, K.A.; Van Wyk, D.R.; Engelhard, M.H.; Wang, C.; Bussell, M.E. Thiophene hydrodesulfurization over nickel phosphide catalysts: Effect of the precursor composition and support. *J. Catal.* **2005**, *231*, 300–313. [CrossRef]
31. Oyama, S.T.; Wang, X.; Lee, Y.K.; Bando, K.; Requejo, F.G. Effect of phosphorus content in nickel phosphide catalysts studied by XAFS and other techniques. *J. Catal.* **2002**, *210*, 207–217. [CrossRef]
32. Koranyi, T.I.; Vit, Z.; Nagy, J.B. Support and pretreatment effects on the hydrotreating activity of SBA-15 and CMK-5 supported nickel phosphide catalysts. *Catal. Today* **2008**, *130*, 80–85. [CrossRef]
33. Zhao, H.Y.; Li, D.; Bui, P.; Oyama, S.T. Hydrodeoxygenation of guaiacol as model compound for pyrolysis oil on transition metal phosphide hydroprocessing catalysts. *Appl. Catal. A Gen.* **2011**, *391*, 305–310. [CrossRef]
34. Prins, R.; Bussell, M. Metal Phosphides: Preparation, Characterization and Catalytic Reactivity. *Catal. Lett.* **2012**, *142*, 1413–1436. [CrossRef]
35. Iino, A.; Cho, A.; Takagaki, A.; Kikuchi, R.; Oyama, S.T. Kinetic studies of hydrodeoxygenation of 2-methyltetrahydrofuran on a Ni_2P/SiO_2 catalyst at medium pressure. *J. Catal.* **2014**, *311*, 17–27. [CrossRef]
36. Landau, M.V.; Herskowitz, M.; Hoffman, T.; Fuks, D.; Liverts, E.; Vingurt, D.; Froumin, N. Ultradeep Hydrodesulfurization and Adsorptive Desulfurization of Diesel Fuel on Metal-Rich Nickel Phosphides. *Ind. Eng. Chem. Res.* **2009**, *48*, 5239–5249. [CrossRef]
37. Wu, S.K.; Lai, P.C.; Lin, Y.C. Atmospheric Hydrodeoxygenation of Guaiacol over Nickel Phosphide Catalysts: Effect of Phosphorus Composition. *Catal. Lett.* **2014**, *144*, 878–889. [CrossRef]
38. Liu, X.G.; Chen, J.X.; Zhang, J.Y. Hydrodechlorination of chlorobenzene over silica-supported nickel phosphide catalysts. *Ind. Eng. Chem. Res.* **2008**, *47*, 5362–5368. [CrossRef]
39. Bekaert, E.; Bernardi, J.; Boyanov, S.; Monconduit, L.; Doublet, M.L.; Menetrier, M. Direct Correlation between the ^{31}P MAS NMR Response and the Electronic Structure of Some Transition Metal Phosphides. *J. Phys. Chem. C* **2008**, *112*, 20481–20490. [CrossRef]
40. Krawietz, T.R.; Lin, P.; Lotterhos, K.E.; Torres, P.D.; Barich, D.H.; Clearfield, A.; Haw, J.F. Solid phosphoric acid catalyst: A multinuclear NMR and theoretical study. *J. Am. Chem. Soc.* **1998**, *120*, 8502–8511. [CrossRef]

41. Eichele, K.; Wasylishen, R.E. ^{31}P NMR Study of Powder and Single-Crystal Samples of Ammonium Dihydrogen Phosphate—Effect of Homonuclear Dipolar Coupling. *J. Phys. Chem.* **1994**, *98*, 3108–3113. [CrossRef]
42. Chen, J.X.; Sun, L.M.; Wang, R.J.; Zhang, J.Y. Hydrodechlorination of Chlorobenzene Over Ni_2P/SiO_2 Catalysts: Influence of Ni_2P Loading. *Catal. Lett.* **2009**, *133*, 346–353. [CrossRef]
43. Cecilia, J.A.; Infantes-Molina, A.; Rodriguez-Castellon, E.; Jimenez-Lopez, A.; Oyama, S.T. Oxygen-removal of dibenzofuran as a model compound in biomass derived bio-oil on nickel phosphide catalysts: Role of phosphorus. *Appl. Catal. B Environ.* **2013**, *136*, 140–149. [CrossRef]
44. Vannice, M.A. Intraphase Gradients (Weisz-Prater Criterion). In *Kinetics of Catalytic Reactions*; Springer Science + Business Media. Inc.: NewYork, NY, USA, 2005; pp. 63–77.
45. Senol, O.I.; Ryymin, E.M.; Viljava, T.R.; Krause, A.O.I. Reactions of methyl heptanoate hydrodeoxygenation on sulphided catalysts. *J. Mol. Catal. A Chem.* **2007**, *268*, 1–8. [CrossRef]
46. JCPDS. *International Centre for Diffraction Data*; JCPDS: Swarthmore, PA, USA, 1997.
47. Furo, I.; Bakonyi, I.; Tompa, K.; Zsoldos, E.; Heinmaa, I.; Alla, M.; Lippmaa, E. ^{31}P Nuclear-Magnetic-Resonance Knight-Shift and Linewidth in Ni_3P and Cu_3P: A Magic-Angle Spinning Study. *J. Phys. Condens. Mat.* **1990**, *2*, 4217–4225. [CrossRef]
48. Andreev, A.S.; de Lacaillerie, J.B.D.; Lapina, O.B.; Gerashenko, A. Thermal stability and hcp-fcc allotropic transformation in supported Co metal catalysts probed near operando by ferromagnetic NMR. *Phys. Chem. Chem. Phys.* **2015**, *17*, 14598–14604. [CrossRef] [PubMed]
49. Wang, X.Q.; Clark, P.; Oyama, S.T. Synthesis, characterization, and hydrotreating activity of several iron group transition metal phosphides. *J. Catal.* **2002**, *208*, 321–331. [CrossRef]
50. Ren, J.; Wang, J.-G.; Li, J.-F.; Li, Y.-W. Density functional theory study on crystal nickel phosphides. *J. Fuel Chem. Technol.* **2007**, *35*, 458–464. [CrossRef]